Structural basis for antagonism of human interleukin 18 by poxvirus interleukin 18-binding protein

Brian Krumm[a], Xiangzhi Meng[b], Yongchao Li[a], Yan Xiang[b,1], and Junpeng Deng[a,2]

[a]Department of Biochemistry and Molecular Biology, Oklahoma State University, Stillwater, OK 74078; and [b]Department of Microbiology and Immunology, University of Texas Health Science Center, 7703 Floyd Curl Drive, San Antonio, TX 78229

Edited by Brian W. Matthews, University of Oregon, Eugene, OR, and approved November 17, 2008 (received for review September 11, 2008)

Human interleukin-18 (hIL-18) is a cytokine that plays an important role in inflammation and host defense against microbes. Its activity is regulated in vivo by a naturally occurring antagonist, the human IL-18-binding protein (IL-18BP). Functional homologs of human IL-18BP are encoded by all orthopoxviruses, including variola virus, the causative agent of smallpox. They contribute to virulence by suppressing IL-18-mediated immune responses. Here, we describe the 2.0-Å resolution crystal structure of an orthopoxvirus IL-18BP, ectromelia virus IL-18BP (ectvIL-18BP), in complex with hIL-18. The hIL-18 structure in the complex shows significant conformational change at the binding interface compared with the structure of ligand-free hIL-18, indicating that the binding is mediated by an induced-fit mechanism. EctvIL-18BP adopts a canonical Ig fold and interacts via one edge of its β-sandwich with 3 cavities on the hIL-18 surface through extensive hydrophobic and hydrogen bonding interactions. Most of the ectvIL-18BP residues that participate in these interactions are conserved in both human and viral homologs, explaining their functional equivalence despite limited sequence homology. EctvIL-18BP blocks a putative receptor-binding site on IL-18, thus preventing IL-18 from engaging its receptor. Our structure provides insights into how IL-18BPs modulate hIL-18 activity. The revealed binding interface provides the basis for rational design of inhibitors against orthopoxvirus IL-18BP (for treating orthopoxvirus infection) or hIL-18 (for treating certain inflammatory and autoimmune diseases).

smallpox | immune evasion | orthopoxvirus | autoimmune disease | inflammatory disease

Interleukin 18 (IL-18) is a proinflammatory cytokine that belongs to IL-1 superfamily (1, 2). It plays an important role in both innate and acquired immune responses, by inducing IFN-γ production from T lymphocytes and macrophages and by enhancing cytotoxicity of natural killer cells (2). IL-18 activity is modulated in vivo by a negative-feedback mechanism involving a naturally occurring IL-18 inhibitor, the IL-18-binding protein (IL-18BP) (3). A functional IL-18BP is also encoded by many poxviruses, including molluscum contagiosum virus (MCV) and orthopoxviruses (4, 5). Orthopoxviruses include several significant human pathogens such as variola virus, which causes smallpox, and monkeypox virus, which is an emerging zoonosis causing a smallpox-like disease in humans (6). IL-18BPs are highly conserved among orthopoxviruses but share only limited homology with that in human. Nevertheless, both human and viral IL-18BPs bind to human IL-18 (hIL-18) extremely strongly with subnanomolar affinity and potently block hIL-18 activity (4, 7, 8). Orthopoxvirus IL-18BP contributes to virulence by down-modulating IL-18-mediated immune responses (5, 9). The mechanism by which IL-18BP inactivates hIL-18 is unclear, but its potent ability to inhibit hIL-18 has prompted an interest in developing IL-18BP as therapeutics (10, 11) because aberrant expression of IL-18 is associated with severe inflammatory conditions, such as some autoimmune diseases. Recombinant human IL-18BP has been shown to be effective at treating inflammatory skin diseases and LPS-induced liver injury (10, 11).

Results and Discussion

Overall Structure of IL-18–Ectromelia Virus (Ectv)IL-18BP Complex. To understand better the molecular basis of IL-18BPs in regulating IL-18 signaling pathway, we crystallized the binary complex of hIL-18 and ectvIL-18BP, which has an essentially identical amino acid sequence as its counterpart in variola virus (with an overall sequence identity of 95%). We determined the complex crystal structure by the single-wavelength anomalous dispersion method. The structure reveals 1 complex per asymmetric unit consisting of a heterodimer of hIL-18 and ectvIL-18BP with a 1:1 stoichiometry (Fig. 1). The complex has overall dimensions of 37 Å × 53 Å × 57 Å with 1 ectvIL-18BP molecule clamping over the top of the hIL-18 β-barrel. The current structure was refined to 2.0-Å resolution with good statistics [supporting information (SI) Table S1].

Structure of EctvIL-18BP. The ectvIL-18BP structure, representing the first structure of any IL-18BPs, adopts a canonical h-type Ig fold, comprising two 4-stranded β-sheets with a very short c′ strand, a short helix (H1), and elongated flexible loops between the β-sheets (Fig. 1 *A* and *B*). The β-sheets are glued together mainly through extensive intersheet hydrophobic interactions. Two disulfide bonds further stabilize the β-sandwich structure of ectvIL-18BP. One of them is formed between a pair of conserved cysteines (Cys-39 and Cys-110) from β-strands b and f, and the other is formed between Cys-25 and Cys-42 from β-strands a and b. The disulfide bonds contribute significantly to the overall integrity of the ectvIL-18BP, noting that the purified complex protein failed to crystallize under reducing conditions. There are only 6 aa that are different between IL-18BPs from ectromelia virus and variola virus. These 6 residues are all surface residues but are mostly not involved in binding IL-18 as shown in our crystal structure (Fig. S1), suggesting that variola virus IL-18BP adopts an essentially identical structure and binds hIL-18 in a manner similar to ectvIL-18BP.

Structure of IL-18. The NMR structure of ligand-free hIL-18 has been reported in ref. 12. Consistent with the NMR structure, the crystal structure of hIL-18 adopts a signature β-trefoil fold, which comprises of 12 β-strands (β1–β12) forming a twisted β-barrel with one short α-helix (H1) and one 3_{10}-helix. The overall crystal structure of hIL-18 closely resembles the NMR structure with an overall rmsd of 1.52 Å over 134 aligned residues

Author contributions: Y.X. and J.D. designed research; B.K., X.M., and Y.L. performed research; B.K., Y.X., and J.D. analyzed data; and B.K., Y.X., and J.D. wrote the paper.

The authors declare no conflict of interest.

This article is a PNAS Direct Submission.

Data deposition: The atomic coordinates and structure factors have been deposited in the Protein Data Bank, www.pdb.org (PDB ID code 3F62).

[1]To whom correspondence may be addressed. E-mail: xiangy@uthscsa.edu.

[2]To whom correspondence may be addressed at: 248 Noble Research Center, Stillwater, OK 74078. E-mail: junpeng.deng@okstate.edu.

This article contains supporting information online at www.pnas.org/cgi/content/full/0809086106/DCSupplemental.

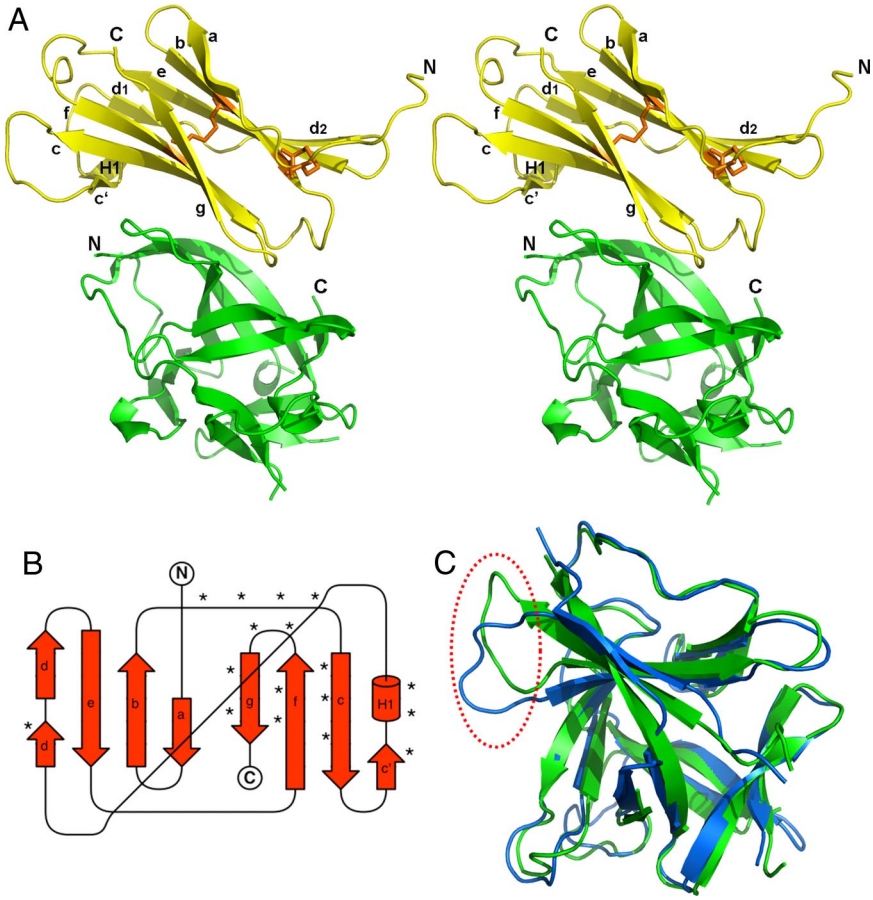

Fig. 1. Overall structure of ectvIL-18BP and hIL-18 complex. (*A*) Stereoview of the complex. EctvIL-18BP (yellow) sits atop the hIL-18 molecule (green), which adopts a β-trefoil structure. The 2 disulfide bonds are shown as orange sticks. The amino and carboxyl termini of the protein polypeptides are indicated as N and C, respectively. EctvIL-18BP adopts a canonical Ig fold whose secondary structures are labeled. (*B*) Topology diagram of ectvIL-18BP. Asterisks indicate the positions of residues interacting with hIL-18. (*C*) Superimposition of the crystal structure of hIL-18 (green) with the ligand-free NMR structure of hIL-18 (blue; PDB ID code 1J0S). Significant conformational changes were observed at the loop region connecting β4 and β5. Notice the loop in the crystal structure shifted by ≈6 Å from its position in ligand-free state, as indicated in a red dashed cycle.

(Fig. 1*C*), but it displays significant conformational changes at the binding interface for IL-18BP (Fig. 2; see below). Missing from the crystal structure of hIL-18 are residues 33–41, which are part of an extended loop between strands β3 and β4, extending from the core of the protein. This suggests that the loop is highly flexible, which is consistent with residues 34–43 being undefined in the NMR structure (12).

EctvIL-18BP Interacts with IL-18 via an Induced-Fit Mechanism. The ectvIL-18BP molecule sits atop the opening of the hIL-18 β-barrel while extending its hydrophobic residues into the β-barrel cavity. Together with complementary residues located on the hIL-18 β-barrel rim, these hydrophobic residues effectively seal off the cavity opening at the complex interface. The complex of hIL-18–ectvIL-18BP buries ≈1,930 Å^2 of solvent-accessible surface area, which is on the upper end of the average area (1,600 ± 400 Å^2) for antibody–antigen interface (13), underscoring the extensive interactions between hIL-18 and ectvIL-18BP. In addition to the extensive hydrophobic interactions, 1 salt bridge, 8 hydrogen bonds, and a strong π-cation interaction are also observed at the interface (Table S2). EctvIL-18BP contributes mainly 17 residues to the complex interface, which are distributed across the hydrophobic back face of the β-sandwich on the β-strands c, c′, d, f, and g, h1 and the loops that connect β-strands b,c and f,g (Figs. 1*B* and 2). These key residues bind to 3 pockets of hIL-18 that we refer to as binding sites A–C (Fig. 2*A*). Most of these key binding residues are conserved among viral and human IL-18BPs despite limited overall sequence identity between human and viral IL-18BPs (Fig. S2). Therefore, the structure of ectvIL-18BP reveals a common structural mechanism for all IL-18BPs to bind hIL-18.

Site A of hIL-18, which mainly comprises 8 surface residues, including Tyr-1, Lys-53, Asp-54, Ser-55, and Pro-57, makes extensive interactions with ectvIL-18BP (Table 1). Strikingly, compared with the NMR solution structure of ligand-free hIL-18, site A in the crystal structure displays a large conformational change, suggesting that the binding is mediated by an induced-fit mechanism. Specifically, upon binding ectvIL-18BP, the N terminus undergoes some remodeling, while the loop between β4 and β5 (residues 54–61) has shifted by nearly 6 Å from its ligand-free position. The conformational changes lead to repositioning of the side chains of Tyr-1, Lys-53, Ser-55, and Pro-57 and create a unique hydrophobic binding pocket absent in the ligand-free hIL-18, making it possible to accommodate Tyr-53 and Phe-67 from ectvIL-18BP (Fig. 2 *B–D* and Fig. S1). The aliphatic side chain of hIL-18 Lys-53 rotates nearly 90° and is entrenched by a wall of hydrophobic side chains composed of Tyr-53 and Phe-67 of ectvIL-18BP and Leu-5 of hIL-18. The positively charged side-chain amino group of hIL-18 Lys-53 forms a strong π-cation interaction with the aromatic ring of ectvIL-18BP Phe-67. Lys-53 also forms a hydrogen bond and a salt bridge, respectively, with Glu-69 and Glu-77 of ectvIL-18BP,

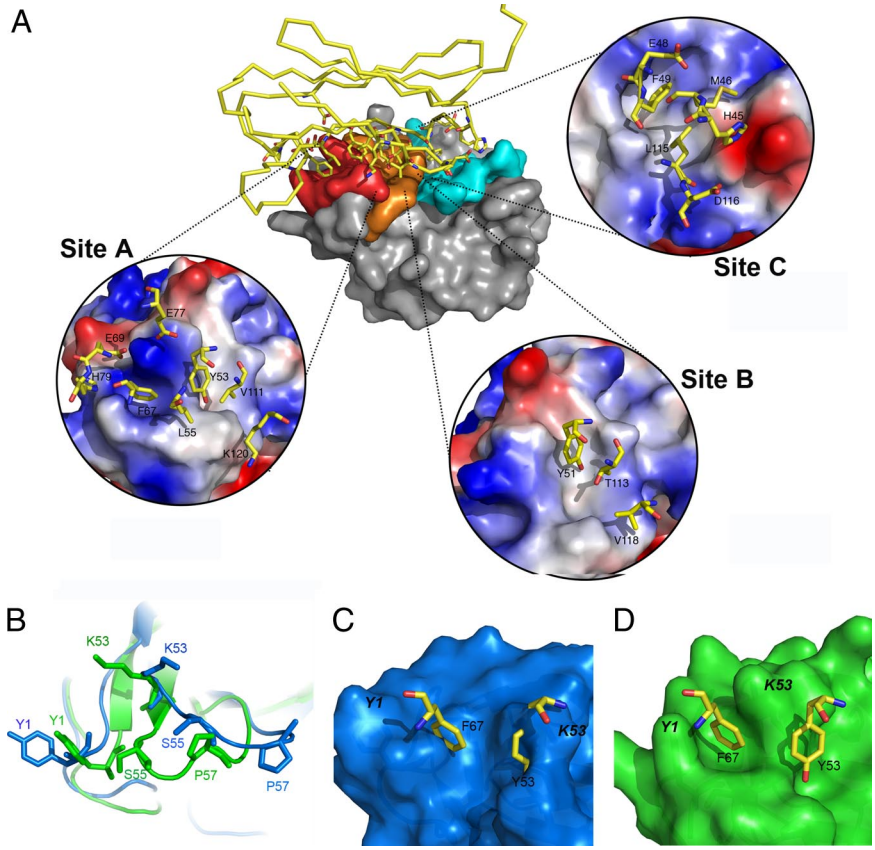

Fig. 2. HIL-18–ectvIL-18BP interface. (*A*) Three binding pockets on hIL-18 surface. (*Center*) EctvIL-18BP and hIL-18 complex in a top-down view as seen in Fig. 1; hIL18 is shown as surface presentation and colored gray, and ectvIL-18BP is drawn as a ribbon diagram with β-sheets colored in yellow. Binding sites A–C on the hIL-18 surface are colored red, orange, and cyan, respectively. EctvIL-18BP residues involved in binding hIL-18 are shown as sticks. (*Insets*) Interactions involved in the respective binding site between ectvIL-18BP and hIL-18. (*B*) Remodeling of hIL-18 at site A. The coloring scheme is the same as in Fig. 1*C*. Tyr-1, Lys-53, Ser-66, and Pro-57 are shown as sticks. Notice the drastic repositioning of the side chains of Tyr-1 and Lys-53 at the carboxyl terminus of hIL-18 upon binding ectvIL-18BP. (*C* and *D*) Results of the conformational change upon ectvIL-18BP binding, yielding a new binding cavity/pocket for Tyr-53 and Phe-67 of ectvIL-18BP (shown as sticks). The ligand-free hIL-18 is shown as a surface presentation in blue in *C*. The complexed hIL-18 in the current crystal structure is shown as surface model in green. Notice that the absence of Phe-67 pocket and the steric clash on Tyr-53 would occur with the ligand-free state of hIL-18. The 2 key hIL-18 residues, Lys-53 and Tyr-1 are labeled as bold italic letters.

effectively lodging hIL-18 Lys-53 into a remarkably secure position. These intimate interactions form a network of stabilizing forces at binding site A, fully explaining some previous mutagenesis studies on various IL-18BPs and hIL-18 (14–17). These studies identified Tyr-53 and Phe-67 of ectvIL-18BP and Lys-53 of hIL-18 as residues that contribute most significantly to complex formation between these 2 molecules. Alanine substitution of these residues or the corresponding residues in human and MCV IL-18BP decreased binding affinity by >100-fold. In addition, a significant but less dramatic decrease in binding affinity resulted from alanine substitutions of Glu-69 and Glu-77 of ectvIL-18BP (or corresponding residues in human or MCV IL-18BP) or Ser-55 and Leu-5 of hIL-18.

Additional conformational changes in site A involve Tyr-1 of hIL-18. The phenol ring of Tyr-1 is repositioned to stack on the edge of ectvIL-18BP Phe-67 and forms a hydrogen bond with the main-chain amide of Phe-67. In addition, the main-chain amide group of Tyr-1 forms an intramolecular hydrogen bond with the side chain of hIL-18 Ser-55. Together with Cβ of Ser-55, Tyr-1 tightly seals off Phe-67 in a deep hydrophobic pocket. The phenol group of Tyr-1 also forms a hydrogen bond with the side chain of His-70 of ectvIL-18BP. This partly explains a previous observation that the side chain of ectvIL-18BP His-70 is critical for binding to hIL-18 but not to murine IL-18 (17) because murine IL-18 contains an Asn instead of a Tyr at position 1. Therefore, Tyr-1 might play an important and species-specific role for hIL18 to bind IL-18BP.

Site B is a large elongated cavity spatially adjacent to site A on the surface of hIL-18 and is mainly constituted of 7 residues that are predominantly hydrophobic (Table 1). The movement of the loop between β4 and β5 in hIL-18 also resulted in remodeling of sites B and C, although to a lesser extent compared with site A. The largest conformational changes were noticed to accommodate the loop connecting β-strands f and g of ectvIL-18BP

Table 1. Residues of hIL-18 and ectvIL-18BP involved at the complex interface

Site	hIL-18	ectvIL-18BP
A	Y1, F2, G3, K53, D54, S55, P57, N91	Y53, L55, F67, E69, H70, E77, V111, K120
B	L5, M51, Y52, R58, G59, M60, A61	Y51, T113, V118
C	K8, I49, V62, Q103, R104, S105, D110, N111, M113, V153	H45, M46, E48, F49, L115, D116

(residues 114–118). Three noncontiguous residues, Tyr-51, Thr-113, and Val-118, from ectvIL-18BP β-strands c, f, and g, reside but do not fully occupy the pocket. Therefore, these 3 residues might contribute very little to overall binding of ectvIL-18BP with hIL-18. Indeed, it was shown by mutagenesis studies that alanine substitution at position Tyr-51 of ectvIL-18BP had negligible effects on hIL-18 binding (17). Although site B appears to be not fully used for the binding with ectvIL-18BP, its large pocket might represent an attractive target for rational design of more effective IL-18 inhibitors.

Site C of hIL-18 is next to site B and comprises mainly 10 surface residues (Table 1). Mainly 4 ectvIL-18BP residues (His-45, Met-46, Phe-49, and Leu-115) from the loops connecting β-strands b,c and f,g, interact with site C predominantly through hydrophobic interactions. EctvIL-18BP Glu-48 is involved in weak van der Waals interactions with hIL18 Lys-8. In addition, the side chain of ectvIL-18BP His-45 forms a hydrogen bond with the side chain of hIL-18 Ser-105, whereas the main-chain carbonyl of ectvIL-18BP Asp-116 is hydrogen bonded with the guanidinium group on the side chain of hIL-18 Arg-104. EctvIL-18BP Phe-49 is inserted into a large hydrophobic pocket at binding site C on hIL-18 (Fig. 2*A*), forming extensive hydrophobic interaction with the wall of the pocket, which is composed of the aliphatic side chains of Lys-8, Met-51, Met-60, Gln-103, Met-113, Val-153, whereas the floor is sealed with the aliphatic side chains of Ile-49 and Val-62. These observations explain previous studies showing that alanine substitution at Phe-49 in ectvIL-18BP (or the corresponding residues in other IL-18BPs) displayed dramatically decreased affinity for hIL-18 (15, 17).

Mechanism of IL-18 Inhibition by EctvIL-18BP. Although the structural basis by which hIL-18 activates its receptor complex (IL-18R) is unclear, it has been proposed that IL-18 binds to IL-18R similarly to the binding of IL-1β to IL-1R, albeit with distinctly different specificities attributable to the different surface properties of the 2 cytokines (12, 18). Previous mutagenesis studies suggested 3 IL-18R-binding sites on hIL-18 (12). Sites I and II were suggested to be involved in IL-18Rα binding, whereas site III was proposed to bind IL-18Rβ. Variola virus IL-18BP has been shown to interact with 3 hIL-18 residues that are part of the site II (16). Human IL-18BP was predicted to interact with the same site based on homology modeling studies (19), therefore suggesting that all IL-18BPs compete with IL-18Rα for site II of hIL-18. Our current complex structure of ectvIL-18BP and hIL-18 supports this mechanism of IL-18 antagonism by providing precise and detailed molecular interactions at the atomic level. The current complex structure identifies ≈25 hIL-18 residues that are involved in ectvIL-18BP binding (Table 1). Six of these residues (Leu-5, Lys-8, Lys-53, Arg-58, Met-60, and Arg-104) were suggested to be part of site II that is involved in IL-18Rα binding (12, 16). Therefore, ectvIL-18BP predominantly blocks the accessibility of the receptor at the putative binding site II on hIL-18 (Fig. 3). EctvIL-18BP appears to also bind hIL-18 in a much deeper and hydrophobic manner in part because several of its hydrophobic residues are protruding into the β-barrel cavity of hIL-18. The current crystal structure displays a 1,930-Å^2 buried solvent-accessible area that is much larger than that observed in the IL-1β–IL-1Rα complex at site II (1,000 Å^2) (18). Assuming that hIL-18 binds its receptor α-subunit in mode similar to that observed in the IL-1β–IL-1Rα complex, our structure suggests a much tighter binding by IL-18BP compared with its receptor, which is further supported by binding studies (8, 15, 16). Therefore, the current structure supports a general inhibition mechanism by which IL-18BP neutralizes hIL-18 through competition with IL-18Rα at a common binding site, thus antagonizing IL-18 and mitigating its effects on IFN-γ production and host immune response.

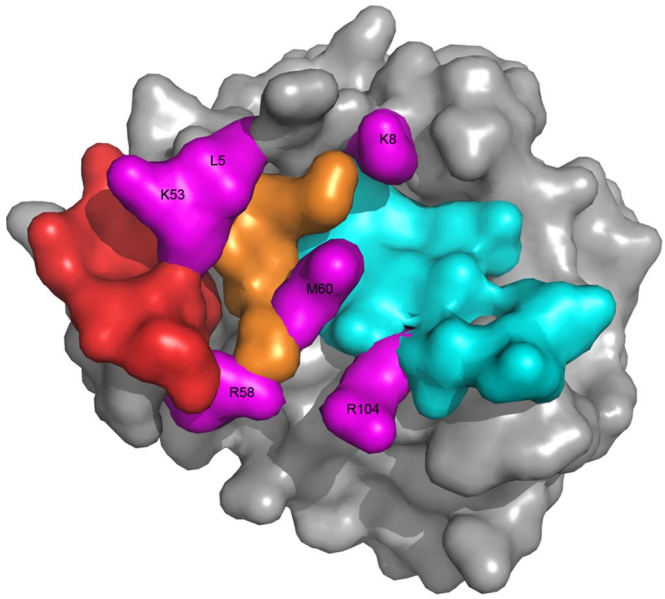

Fig. 3. Mechanism by which ectvIL-18BP inhibits hIL-18. EctvIL-18BP blocks the putative hIL-18Rα-binding site. Human IL-18 is represented as a surface model as viewed from the top of the β-trefoil. EctvIL-18BP-binding sites A–C on hIL-18 are colored in red, orange, and cyan, respectively. Human IL-18 residues that are potentially shared between ectvIL-18BP and hIL-18Rα are colored in purple and span the 3 ectvIL-18BP-binding sites on hIL-18.

Implications of the Structure on Drug Design. Inhibitors against IL-18 are promising pharmaceuticals against some autoimmune and inflammatory diseases where IL-18 activity plays a significant role. Inhibitors against poxvirus IL-18BP could also have significant pharmaceutical potential in treating orthopoxvirus diseases. In fact, it was recently reported that immune response to type I IFN-binding protein of ECTV, which is another secreted poxvirus immune modulator, protects mice from lethal mousepox (20). The revealed unique binding pockets at the ectvIL-18BP–hIL-18 interface provide an invaluable platform for developing these inhibitors.

Methods

Protein Purification and Crystallization. A bicistronic expression vector of ectvIL-18BP and hIL-18 was constructed as follows by using a modified pET28b vector that expresses maltose-binding protein (MBP) with an N-terminal 6-histidine tag and a C-terminal tobacco etch virus (TEV) protease recognition site (ENLYFQG). First, the coding sequence for mature ectvIL-18BP (residues 21–126) was cloned in-frame 3′ to the TEV protease cleavage site. Second, a cassette containing the coding sequence for mature hIL-18 (residues 37–193) under the control of a T7 promoter was inserted into the vector. His_6-MBP-ectvIL-18BP fusion protein and hIL-18, under the control of 2 separate T7 promoters, were coexpressed by the bicistronic expression vector in *Escherichia coli* BL21 (DE3) cells. To decrease nonspecific intermolecular disulfide bond formation, a mutant hIL-18 containing 4 Cys/Ser substitutions (4S) was constructed as described in ref. 21 and cloned into a similar bicistronic expression vector. The complex was purified by using a procedure similar to that described in ref. 22. Briefly, the protein complex was copurified first from the soluble cell lysates with a Ni-nitrilotriacetic acid (NTA) affinity column. The eluted proteins were subjected to TEV protease cleavage, and the ectvIL-18BP–hIL-18 protein complex was collected as the flow-through of a second Ni-NTA column. The protein complex was further purified through size exclusion chromatography with a Superdex 200 column, which indicated a 1:1 molar ratio stoichiometry. The ectvIL-18BP and hIL-18 protein complex was concentrated to 9 mg/mL, then flash frozen and stored at −80 °C until usage (23). The complex crystallized in a condition containing 30% PEG 3350, 0.5 M KCl, and 0.1 M sodium citrate (pH 4.5). Twenty percent (vol/vol) glycerol was added to the mother liquid as cryoprotectant.

Structure Determination. A set of data was collected on a selenomethionine (SeMet)-substituted crystal at beamline 19-ID at the Advanced Photon Source, Argonne National Laboratory. The structure was solved by the single-wavelength anomalous dispersion method by using HKL3000 (24). Autotracing by Arp/Warp (25) yielded a nearly complete model. The SeMet-phased model was used to solve the native structure of mutant 4S by the molecular replacement method using phaser (26). The complex structures of native and SeMet-substituted proteins are essentially identical, therefore only the native structure was discussed in this article. REFMAC5 (27) was used for refinement, and Coot (28) was used for iterative manual model building. The structure was refined to 2.0-Å resolution with R_{work} and R_{free} of 18.9% and 23.5%, respectively. Translation, libration, and screw-rotation displacement (TLS) groups used in the refinement were defined by the TLMSD server (29). All molecular graphic figures were generated with PyMOL (30).

ACKNOWLEDGMENTS. We thank the staff of beamline 19ID at the Advanced Photon Source for their support. This work was supported by the Division of Agricultural Sciences and Natural Resources at Oklahoma State University (J.D.) and by National Institutes of Health Grant AI079217 (to Y.X.).

1. Okamura H, *et al.* (1995) Cloning of a new cytokine that induces IFN-γ production by T cells. *Nature* 378:88–91.
2. Dinarello CA (1999) Interleukin-18. *Methods* 19:121–132.
3. Novick D, *et al.* (1999) Interleukin-18-binding protein: A novel modulator of the Th1 cytokine response. *Immunity* 10:127–136.
4. Xiang Y, Moss B (1999) IL-18 binding and inhibition of interferon γ induction by human poxvirus-encoded proteins. *Proc Natl Acad Sci USA* 96:11537–11542.
5. Born TL, *et al.* (2000) A poxvirus protein that binds to and inactivates IL-18 and inhibits NK cell response. *J Immunol* 164:3246–3254.
6. Parker S, Nuara A, Buller RM, Schultz DA (2007) Human monkeypox: An emerging zoonotic disease. *Future Microbiol* 2:17–34.
7. Calderara S, Xiang Y, Moss B (2001) Orthopoxvirus IL-18-binding proteins: Affinities and antagonist activities. *Virology* 279:22–26.
8. Kim SH, *et al.* (2000) Structural requirements of six naturally occurring isoforms of the IL-18-binding protein to inhibit IL-18. *Proc Natl Acad Sci USA* 97:1190–1195.
9. Reading PC, Smith GL (2003) Vaccinia virus interleukin-18-binding protein promotes virulence by reducing γ interferon production and natural killer and T cell activity. *J Virol* 77:9960–9968.
10. Faggioni R, *et al.* (2001) IL-18-binding protein protects against lipopolysaccharide-induced lethality and prevents the development of Fas/Fas ligand-mediated models of liver disease in mice. *J Immunol* 167:5913–5920.
11. Plitz T, *et al.* (2003) IL-18-binding protein protects against contact hypersensitivity. *J Immunol* 171:1164–1171.
12. Kato Z, *et al.* (2003) The structure and binding mode of interleukin-18. *Nat Struct Biol* 10:966–971.
13. Lo Conte L, Chothia C, Janin J (1999) The atomic structure of protein–protein recognition sites. *J Mol Biol* 285:2177–2198.
14. Xiang Y, Moss B (2001) Correspondence of the functional epitopes of poxvirus and human interleukin-18-binding proteins. *J Virol* 75:9947–9954.
15. Xiang Y, Moss B (2001) Determination of the functional epitopes of human interleukin-18-binding protein by site-directed mutagenesis. *J Biol Chem* 276:17380–17386.
16. Meng X, Leman M, Xiang Y (2007) Variola virus IL-18-binding protein interacts with three human IL-18 residues that are part of a binding site for human IL-18 receptor α subunit. *Virology* 358:211–220.
17. Esteban DJ, Buller RM (2004) Identification of residues in an orthopoxvirus interleukin-18-binding protein involved in ligand binding and species specificity. *Virology* 323:197–207.
18. Vigers GP, Anderson LJ, Caffes P, Brandhuber BJ (1997) Crystal structure of the type I interleukin-1 receptor complexed with interleukin-1β. *Nature* 386:190–194.
19. Kimura T, *et al.* (2008) Expression, purification, and structural analysis of human IL-18-binding protein: A potent therapeutic molecule for allergy. *Allergol Int* 57:367–376.
20. Xu RH, *et al.* (2008) The orthopoxvirus type I IFN-binding protein is essential for virulence and an effective target for vaccination. *J Exp Med* 205:981–992.
21. Yamamoto Y, *et al.* (2004) Generation of highly stable IL-18 based on a ligand–receptor complex structure. *Biochem Biophys Res Commun* 317:181–186.
22. Deng J, *et al.* (2008) Structure of the ROC domain from the Parkinson's disease-associated leucine-rich repeat kinase 2 reveals a dimeric GTPase. *Proc Natl Acad Sci USA* 105:1499–1504.
23. Deng J, *et al.* (2004) An improved protocol for rapid freezing of protein samples for long-term storage. *Acta Crystallogr D* 60:203–204.
24. Minor W, Cymborowski M, Otwinowski Z, Chruszcz M (2006) HKL-3000, the integration of data reduction and structure solution: From diffraction images to an initial model in minutes. *Acta Crystallogr D* 62:859–866.
25. Collaborative Computational Project N (1994) The CCP4 Suite: Programs for Protein Crystallography. *Acta Crystallogr D* 50:760–763.
26. McCoy AJ, *et al.* (2007) Phaser crystallographic software. *J Appl Crystallogr* 40:658–674.
27. Murshudov GN, Vagin AA, Dodson EJ (1997) Refinement of macromolecular structures by the maximum-likelihood method. *Acta Crystallogr D* 53:240–255.
28. Emsley P, Cowtan K (2004) Coot: model building tools for molecular graphics. *Acta Crystallogr D* 60:2126–2132.
29. Painter J, Merritt EA (2006) Optimal description of a protein structure in terms of multiple groups undergoing TLS motion. *Acta Crystallogr D* 62:439–450.
30. DeLano WL (2002) The PyMOL Molecular Graphics System (DeLano Scientific, Palo Alto, CA).